Contents lists available at ScienceDirect

Osteoarthritis and Cartilage Open

Laser-irradiating infrared attenuated total reflection spectroscopy of articular cartilage: Potential and challenges for diagnosing osteoarthritis

P. Krebs [a], M. Nägele [b], P. Fomina [a], V. Virtanen [c], E. Nippolainen [d], R. Shaikh [d], I.O. Afara [d], J. Töyräs [d,e,f], I. Usenov [g], T. Sakharova [g], V. Artyushenko [g], V. Tafintseva [h], J.H. Solheim [h], B. Zimmermann [h], A. Kohler [h], O. König [i], S. Saarakkala [c,j], B. Mizaikoff [a,k,*]

[a] *Institute of Analytical and Bioanalytical Chemistry, Ulm University, Ulm, Germany*
[b] *OptoPrecision GmbH, Bremen, Germany*
[c] *Research Unit of Health Sciences and Technology, Faculty of Medicine, University of Oulu, Oulu, Finland*
[d] *Department of Technical Physics, University of Eastern Finland, Kuopio, Finland*
[e] *Science Service Center, Kuopio University Hospital, Kuopio, Finland*
[f] *School of Electrical Engineering and Computer Science, The University of Queensland, Brisbane, Australia*
[g] *Art Photonics GmbH, Berlin, Germany*
[h] *Faculty of Science and Technology, Norwegian University of Life Sciences, Ås, Norway*
[i] *Nanoplus Advanced Photonics Gerbrunn GmbH, Gerbrunn, Germany*
[j] *Department of Diagnostic Radiology, Oulu University Hospital, Oulu, Finland*
[k] *Hahn-Schickard, Ulm, Germany*

ARTICLE INFO

ABSTRACT

Objective: A prototype infrared attenuated total reflection (IR-ATR) laser spectroscopic system designed for *in vivo* classification of human cartilage tissue according to its histological health status during arthroscopic surgery is presented. Prior to real-world *in vivo* applications, this so-called osteoarthritis (OA) scanner has been tested at *in vitro* conditions revealing the challenges associated with complex sample matrices and the accordingly obtained sparse spectral datasets.

Methods: In vitro studies on human knee cartilage samples at different contact pressures (i.e., 0.2–0.5 MPa) allowed recording cartilage degeneration characteristic IR signatures comparable to *in vivo* conditions with high temporal resolution. Afterwards, the cartilage samples were assessed based on the clinically acknowledged osteoarthritis cartilage histopathology assessment (OARSI) system and correlated with the obtained sparse IR data.

Results: Amide and carbohydrate signal behavior was observed to be almost identical between the obtained sparse IR data and previously measured FTIR data used for sparse partial least squares discriminant analysis (SPLSDA) to identify the spectral regions relevant to cartilage condition. Contact pressures between 0.3 and 0.4 MPa seem to provide the best sparse IR spectra for cylindrical (d = 3 mm) probe tips.

Conclusion: Laser-irradiating IR-ATR spectroscopy is a promising analytical technique for future arthroscopic applications to differentiate healthy and osteoarthritic cartilage tissue. However, this study also revealed that the flexible connection between the laser-based analyzer and the arthroscopic ATR-probe via IR-transparent fiber-optic cables may affect the robustness of the obtained IR data and requires further improvements.

1. Introduction

Osteoarthritis (OA) is a worldwide occurring disease, that usually becomes evident at an advanced age by onset-up pain, morning stiffness and a reduced joint load capacity resulting from the abrasion of cartilage in the joints [1,2]. Besides the increasing abrasion of cartilage tissue with age, cartilage injuries due to accidents can also lead to a degenerative joint condition known as posttraumatic osteoarthritis [3,4]. A particular challenge is the fact that between an outbreak and the actual diagnosis of the disease an average period of decades may have passed [5,6]. This

---

may be primarily attributed to current diagnostic methods such as physical examination (e.g. mobility examination of the joint, analysis of gait and movement disorders, etc.) or imaging techniques (e.g. computed tomography, magnetic resonance imaging), which only provide results once the protective cartilage has already severely degenerated and the functionality of the cartilage tissue/joint is significantly affected [7–11]. Early detection of potentially detrimental changes in cartilage tissue enables a variety of treatment options such as cartilage repair surgery, while extensive degeneration in later stages usually require replacement of the entire joint with an artificial prosthesis [12–15]. Due to the limited self-repair of the articular cartilage tissue, which is probably related to low metabolic activity and low blood transport [4,16], arthroscopic interventions with resections are performed conservatively. Consequently, it is evident that a more profound understanding of disease development and progression together with new monitoring modalities, which also enable the spot detection of early detrimental changes within arthroscopic interventions, could enable new options and strategies for the treatment of osteoarthritis.

A promising analytical technique for addressing complex tissue samples such as articular cartilage in a non-destructive way is infrared attenuated total reflection (IR-ATR) spectroscopy [17,18]. In brief, the mid-infrared spectral range (3–15 μm wavelengths) provides unique spectroscopic signatures (i.e. 'molecular fingerprints') of almost any kind of organic and/or inorganic molecules even in complex samples [19]. In IR-ATR spectroscopy, rather than directly illuminating the sample light is propagated via a high-refractive-index waveguide (i.e. ATR element) acting as the active sensing interface with an evanescent field penetrating into a low-refractive-index sample contacted with the transducer [20]. Using evanescent field absorption, an IR-spectrum can be recorded accordingly. A unique feature of IR-ATR spectroscopy is that rather opaque samples that in transmission-absorption would result in total radiation absorbance such as aqueous media or samples containing water (e.g., tissues) may be probed, as the evanescent field leaks exponentially decaying in intensity only a few micrometers into the sample [21]. Since the technique does not require any sample preparation, cartilage tissue can be examined directly in its native state, non-destructively and therefore potentially also *in vivo*, if the measurement technique is provided in an endoscopic format. Moreover, in IR-ATR spectroscopy the morphology of the sample surface is negligible, especially in the case of soft/semi-soft samples such as cartilage, if a sufficient contact area between the sample and the sensor element is ensured [22]. Thus, this technology is ideally suited for medical screening applications if evolved into an insertable endoscopic probe-type format, as shown in the present study. Another advantage of infrared spectroscopy is the detailed molecular information obtained in the so fingerprint regime ($<1500 \text{ cm}^{-1}$), as the excitation of characteristic fundamental and combinatorial molecular vibrations facilitate the direct label-free identification of molecules, if their signals is sufficiently differentiated from the signature of the sample matrix [19,23]. If the sample matrix is more complex and direct extraction of the target analyte signature is not possible, multivariate statistical methods (i.e. chemometrics) may be applied for obtaining quantitative information even from complex samples [24,25]. Articular cartilage (AC) including knee joint cartilage, consists of 65–80 wt% of tissue fluid, which is mainly composed of water [26]. The remaining dry material of AC tissue comprises collagens (70%), proteoglycans (20%) with additional albeit minor contributions of matrix proteins (10%) and lipids [27,28]. Considering this rather manageable number of primary tissue components, the basis of the present study is the hypothesis that it should be possible to assess the tissue condition using a limited set of individual wavelengths within the mid-infrared band in lieu of the entire IR spectrum, which allows for the application of high-performance distributed feedback quantum-cascade lasers (DFB-QCL) spectroscopy instead of a conventional broadband FTIR techniques.

Consequently, the present study discusses a prototype DFB-QCL-based laser spectroscopic sensor system in an endoscope format

combined with an IR-ATR probe for future *in vivo* applications during arthroscopic surgery. The fundamental utility of this tool is demonstrated herein via contact-pressure-controlled measurements at human knee cartilage plugs and verified via IR-ATR using a conventional FTIR spectrometer. The investigated human cartilage samples were examined histologically after the IR measurements and classified via the osteoarthritis cartilage histopathology assessment (OARSI) system. The obtained results are encouraging and demonstrate a distinct correlation between the IR spectral data and the histological condition of the cartilage tissue, using a set of discrete IR wavelengths in lieu of a full spectrum. Considering that this is a preliminary study, and that the OA scanner is at a prototype level, the obtained results are promising, while also revealing challenges and improvements required prior to more extensive *in vitro* studies, and finally, *in vivo* testing in real-world clinical scenarios. Nevertheless, a solid foundation for laser-based IR-ATR spectroscopy in an endoscopic format serving as a promising tool for future real-time *in vivo* monitoring and screening applications has been established.

2. Methods

2.1. IR-spectroscopic osteoarthritis scanner prototype

Generally, the OA scanner prototype comprises two essential components: (i) the main laser unit, and (ii) the IR-ATR probe (Fig. 1). The main unit contains seven specifically developed fiber-coupled DFB-QCLs (nanoplus Advanced Photonics Gerbrunn GmbH, Gerbrunn, Germany) that emit at relevant wavelengths previously selected in the course of this study using sparse partial least squares discriminant analysis (SPLSDA) modelling approach (for more details see supplementary information). Due to the prototype level of the device, minor deviations from the wavelengths from the SPLSDA analyses occurred. The laser wavelengths of the OA scanner, the wavelengths resulting from the SPLSDA analyses and possible cartilage-relevant molecular structures that are crucial for distinguishing the health condition are listed in Table 1. Exemplary broadband IR spectra of cartilage tissue and the laser set of the AO scanner are shown in Fig. 2. Here, it is also evident that the IR signal of the bending vibration of water overlaps with the amide I and II bands. Hence, the lasers at 1606 cm^{-1} and 1581 cm^{-1} are also sensitive to changes of water content within the AC tissue.

A so-called 'fiber spider' comprising a bundle of seven individual polycrystalline infrared-transparent (PIR) fibers based on AgCl/AgBr was developed (art photonics GmbH, Berlin, Germany), each coupled to an individual laser, and merged into a single output fiber serving as an efficient beam combiner. Due to the flexibility of the PIR fibers, the fiber spider enables a flexible arrangement of the laser heads within the main unit such that a compact device footprint (50 cm × 50 cm × 30 cm) is maintained. Devices with such a number of laser heads usually require bulky and complex mirror optics, which are not required in the OA
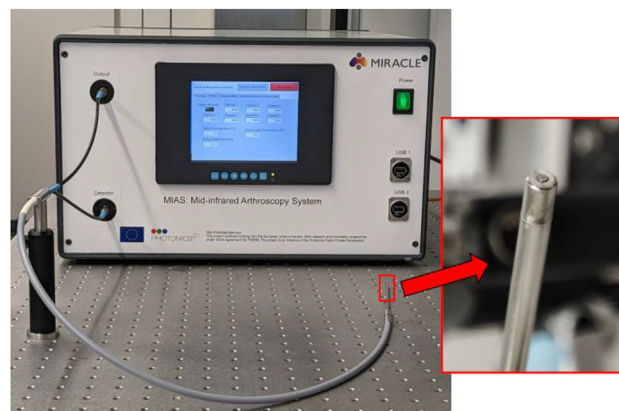

Fig. 1. AO scanner prototype with connected diamond IR-ATR probe.

Table 1
Overview of wavelengths of the OA scanner and the relevant wavelengths from the SPLSDA analyses including relevant molecular structures in AC tissue that are addressed and/or the intended purpose of the wavelengths.

Wavenumber [cm^{-1}]		Targeted IR oscillation/s or purpose	Reference/s
OA scanner	SPLSDA		
1799	1800	Baseline	
1745	1745	C=O stretching (lipids)	[29]
1606	1620	C=O stretching (amide I)	[29–31]
1581	1560	C–N stretching (amide II)	[29–31]
		N–H bending (amide II)	[29–31]
		C–C stretching (amide II)	[31]
1207	1210	C–N stretching (amide III)	[30,31]
		N–H bending (amide III)	[30,31]
1084	1080	C–O stretching (carbohydrates)	[29]
		Ring vibrations (carbohydrates)	[31]
880	850	Water librations; Normalization[a]	[32,33]

[a] Possible cross-sensitivities (due to protein or amino acid signals) under the librational band of water were not considered, since the subsequent performance of the OA scanner system could not be clearly estimated.
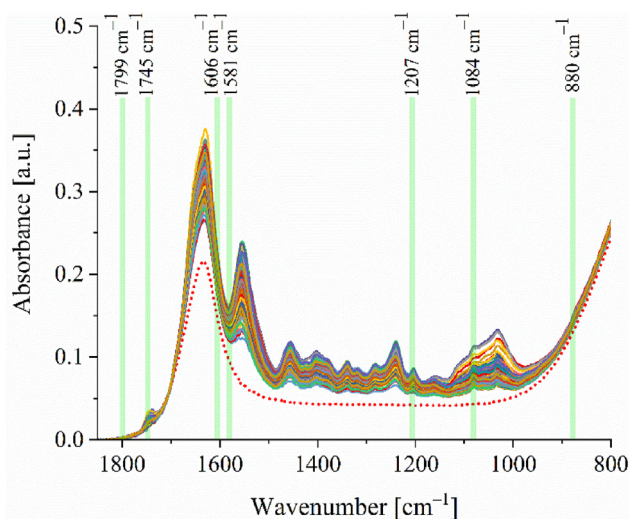
Fig. 2. Selected laser wavelengths of the AO scanner shown on FTIR spectra of human AC tissue. The red dotted line shows a water spectrum indicating the spectral regions where water overlaps with the amide features. (Lipid: 1745 cm^{-1}; amide I/water: 1606 cm^{-1}; amide II/water: 1581 cm^{-1}; amide III: 1207 cm^{-1}; carbohydrate: 1084 cm^{-1}; background/baseline: 1799 cm^{-1}, 880 cm^{-1}).

scanner system developed herein. The IR radiation from the PIR fiber spider is then focused via an off-axis parabolic (OAP) mirror into the arthroscopic IR-ATR probe – or any other transducer system – via a standard F-SMA connector. A thermoelectrically cooled mercury cadmium telluride (MCT) detector was used to record the resulting analytical signals coupled into the device via a second F-SMA-connector. Next to custom QCLs and the PIR fiber spider, also the electronic control of the laser drivers in combination with the analog-to-digital data acquisition of the MCT detector signal was customized (OptoPrecision GmbH, Bremen, Germany) and designed such that a single detector records all seven laser signals in a time-gated sequence, which enables using a single detector despite seven light sources are applied. Individual laser signals were averaged across 20 pulses in 0.1 s. Hence, after approximately 0.7 s a sparse data set containing the spectral information at the seven wavelengths can be obtained. The signals can be read out directly via a processing unit implemented within the OA scanner and the data can be visualized essentially in real time via an integrated screen at the front panel of the device. It should be noted that the modular design of the main unit facilitates a wide range of combinations with alternative sensors, probes or sampling interfaces and application scenarios with the

laser wavelengths tailored to the specific use case. The arthroscopic ATR-probe (art photonics GmbH) again consisted of PIR fibers capped by a hemispherical diamond ATR sensor element with a surface area of approximately 0.45 mm^2, which is in contact with the actual cartilage sample. The ATR-probe shaft diameter was 3 mm with a shaft length of 12 cm made from medical-grade Hastelloy C22. The fiberoptic cable length connecting the main unit with the ATR probe was 70 cm.

2.2. Human cartilage sample extraction and storage

Human cartilage samples ($n = 54$; sample diameter $d = 4$ mm) were harvested from 4 cadaver donors obtained from a commercial biobank (Science Care, USA). The samples were prepared by drilling cylindrical 4 mm osteochondral plugs with a dental drill from the central locations of femoral, tibial and patellar cartilage. The samples were doused with water during drilling operation to prevent overheating. The extracted cartilage plugs were stored in 1.8 mL cryotubes filled with phosphate-buffered saline solution. The solution was prepared by mixing 1.44 g Na$_2$HPO$_4$, 0.24 g KH$_2$PO$_4$, 8 g NaCl and 0.2 g KCl in 800 mL deionized water. The samples were stored frozen (-80 °C) to avoid/reduce the effects of biological and physical degradation. The cartilage samples were only thawed for the IR measurements and histological examination ensuring that the human cartilage samples are in pristine biophysical condition. The study was approved by the Research Ethics Committee of the Northern Savo Hospital District (Kuopio University Hospital, Kuopio, Finland, permission #134/2015).

2.3. Sample preparation for IR measurements

For measurements of cartilage tissue, the samples ($n = 54$) were prepared such that the cartilage surface could be brought into contact with the surface of IR-ATR sensor. It was important that both surfaces were aligned parallel to each other ensuring optimum contact. The bone ends of the 4 mm cylindrical cartilage plugs were cut with a scalpel and clamped to suitable sample holders (see supplementary information). Special care was taken to ensure that the contact with the sample holder was only maintained via the bone section of the cartilage plug and that the cartilage tissue was not affected by any force or tension caused by mounting within the holder. The samples were deliberately not fixed with isocyanate glue, because contamination of the tissue surfaces by glue could lead to falsified IR signals, as IR-ATR spectroscopy is particularly surface sensitive. The sample holder was filled with Ringer's solution (RS; B. Braun Melsungen AG, Melsungen, Germany), a commonly used flushing fluid in surgery for avoiding cartilage surface drying and maintaining the initial AC condition during the experiments [34]. Thus, it was ensured that the *in vitro* setting for the cartilage measurements resembles the *in vivo* scenario as close as possible, i.e., a minimally invasive arthroscopic examination of cartilage in the knee joint.

2.4. OA scanner prototype measurement parameters

Due to signal fluctuations induced by fiber movement during the first tests, all experiments were performed with a mechanically fixed IR-ATR probe. Using an x-y-z positioner, the sample could be moved towards the probe and at the same time the contact pressure could be accurately controlled via a FH-2000 balance (G&G GmbH, Kaarst, Germany) mounted on top of the positioner. At the beginning of each IR measurement, a background of air was measured for 3 min. Subsequently, the tip of the IR-ATR probe was immersed in RS for 3 min. A cartilage sample was then analyzed for 40 s with a specified contact pressure between the probe and the cartilage sample. After 40 s, the pressure was released, the probe was completely removed from the cartilage surface, and the tissue was allowed to relax for 40 s. Then, the same experiment was executed at an incremental increase of the contact pressure. Pressure steps of 0.2 MPa, 0.3 MPa, 0.4 MPa, and 0.5 MPa were executed. (These relatively modest pressure steps are significantly below the dynamic modulus and

below/low aggregate modulus of AC. This ensures that damage to cartilage tissue samples caused by the measurement procedure itself is minimal and during the compression just some loss of tissue free water can occur) [35]. Each pressure step was repeated 3 times. At the end of each pressure step, the RS was again analyzed for 3 min.

2.5. IR-ATR measurements with conventional FTIR

Reference data for the OA scanner prototype were recorded using a Bruker Vertex 70 FTIR spectrometer (Bruker Optics GmbH & Co. KG., Ettlingen, Germany) equipped with a nitrogen cooled MCT detector and a GladiATR ATR assembly (PIKE Technologies, Madison, USA). This ATR system comprises a single-bounce diamond ATR element and a stamp with an integrated pressure sensor. First, RS spectra were recorded followed by a cartilage sample placed into the RS and pressed against the diamond ATR surface for approx. 40 s. Thereafter, the cartilage sample was removed from the surface such that the sample could relax for approximately 40 s in RS. Again, three different pressure steps (0.2 MPa, 0.4 MPa and 0.5 MPa) were executed 3 times. All spectra were recorded at a spectral resolution of 2 cm^{-1} averaging 32 scans in the spectral range 4000–600 cm^{-1}. These measurement parameters were optimized such that six spectra could be recorded within the same time period as with the OA scanner, i.e., approximately within 40 s.

2.6. Histological evaluation

After IR measurements, cartilage samples were fixed in formalin, decalcified in ethylenediaminetetraacetic acid, and embedded in paraffin. 9 histological sections (thickness = 3 μm) of each sample were cut and stained using Safranin-O, which binds stoichiometrically to the matrix proteoglycans. Additionally, digital images were acquired from each histological section using a PathScanEnabler-IV (Meyer Instruments, Inc., Houston, USA). The digital images were initially independently examined by three graders using the OARSI system. Afterwards, the results were brought to a consensus within a discussion group of all graders to ensure consistent evaluation results. For subsequent correlation with the IR data, the cartilage samples were classified according to the following criteria: healthy (OARSI: 0–1.5), intermediate deterioration (OARSI: 2–2.5), and severely damaged (OARSI: 3 and higher).

2.7. Data analysis

A detailed explanation of how the raw data of the OA scanner looks like and how the information of the cartilage tissue samples was extracted is explained in the supplementary information. All cartilage data had to be analyzed with respect to all single laser signal changes and as an entire laser set ensemble ("sparse spectra"). Data indicating no/less contact between AC and probe, a larger cartilage damage within the measurement or an entire irregular sparse spectrum (caused by the spatially distributed evanescent field spots of the lasers) were excluded. The cleansed data were sorted according to their OARSI grading results and median values were calculated to obtain signal progression plots which give insights into the individual behaviors of healthy, intermediate and damaged classified cartilage tissue measured via OA scanner applying different contact pressures with the ATR probe.

2.8. Software

Within the OA scanner prototype, the data were recorded via a LabVIEW based program (MIRACLE V2.1.16, OptoPrecision, Bremen, Germany). Likewise, data processing was performed by a custom program (MIRACLE data viewer and labeling tool V2.3, OptoPrecision, Bremen, Germany). The spectra recorded using the conventional FTIR system were processed using the OPUS 8.1 software package (Bruker Optics GmbH & Co. KG., Ettlingen, Germany).

3. Results

The final data set consists of 139 measurements considering 52 cartilage plugs for 0.2 MPa contact pressure, 106 measurements considering 39 cartilage plugs for 0.3 MPa contact pressure, 101 measurements considering 37 cartilage plugs for 0.4 MPa contact pressure and 89 measurements considering 32 cartilage plugs for 0.5 MPa contact pressure. Fig. 3 shows all median curve progressions of the signals of the lipid, amide, and carbohydrate lasers under the various pressure steps and different cartilage conditions (healthy, intermediate, and damaged). The characteristic fin-like signal structures of amide and carbohydrate lasers indicating the visco-elastic behavior of the AC tissue and responds time-depended to the contact pressure applied via the probe [26,36,37]. Simultaneously, it can be observed that the signals from these lasers increase continuously over time. Only the lipid laser signals at 1745 cm^{-1} showed a rather step-like signal curve, which settled after about 20 s, indicating a very surface-specific lipid distribution within the AC tissue.

Regarding the cartilage health conditions, it can be observed that the amide signals (1606 cm^{-1}, 1581 cm^{-1} and 1207 cm^{-1}) decrease with increasing cartilage degeneration, while lipid (1745 cm^{-1}) and carbohydrate signals (1084 cm^{-1}) increase with increasing degeneration. The amide signals at 1606 cm^{-1} and 1581 cm^{-1} are significantly more intense than the signal at 1207 cm^{-1}. Since water overlaps with the amide signals at 1606 cm^{-1} and 1581 cm^{-1} (see Fig. 2), a decreasing water content with increasing cartilage degeneration can also be expected. All observations are largely consistent with the FTIR preliminary tests performed for the SPLSDA analyses. Only the lipid signal shows inconsistencies. According to the SPLSDA analysis, the lipid signal should decrease with increasing cartilage degeneration.

The ideal contact pressure of a probe with a 3 mm cylindrical probe head is between 0.3 MPa and 0.4 MPa. Contact pressures of 0.2 MPa result in no separation of the individual cartilage health conditions for the lipid and carbohydrate signals. A delayed separation between healthy and intermediate condition occurs with the amide signals. At 0.3 MPa, a proper separation between healthy, intermediate and damaged condition can be observed for the amide signals. Lipid and carbohydrate signals also indicate initial separations. At 0.4 MPa, the separation behavior of the amide signals at 1606 cm^{-1} and 1581 cm^{-1} is similar to the separation behavior at 0.3 MPa. This could be the first indication of contact saturation between the cartilage samples and the probe. Lipid and carbohydrate signals now also show good separation behavior of the different cartilage conditions. The separation capacity of the amide signal at 1207 cm^{-1} seems to collapse. At pressures of 0.5 MPa, the amide signals at 1606 cm^{-1} and 1581 cm^{-1} show delayed separations of intermediate and damaged cartilage states. Lipid and carbohydrate signals indicate a more efficient separation between the cartilage conditions. The collapse of the separation capacity of the amide signals and the increasing separation capacity by the carbohydrate signal may indicate the first signs of cartilage tissue damage caused by the probe.

4. Discussion

This work indicates the potential of laser-irradiated infrared attenuated total reflectance spectroscopy for clinical applications, since the laser signals provide not only spectral information, but also direct feedback on the contact between sample and probe. Since the temporal resolution of laser-based systems is far higher than that of FTIR systems, new options for spectral investigation methods arise. Events such as relaxation of the sample tissue, tissue cracks, etc. can be better examined/identified due to the associated speed of the measurements and enables the surgeon to obtain feedback in near real time in arthroscopic applications. In the case of AC tissue, the progression curves of the various health conditions indicate that information on possible tissue changes can be obtained within just a few seconds. Hence, it can be stated that laser-irradiated infrared attenuated total reflectance spectroscopy of cartilage has theoretical potential for diagnosing cartilage degeneration. However, several

technical challenges were identified, which must be improved and/or optimized prior to clinical testing. An important aspect is improving the coupling efficiency and robustness of the optical alignment of the 7 QCLs vs. the PIR fiber facet of the probe. The beam pattern illuminates only parts of the incoupling fiber facet of the IR-ATR probe creating an associated propagating mode pattern, which changes if the IR-ATR probe is moved. Likewise, returning the probe to the initial position after a measurement does not yield the initial laser intensity values. Hence, it is anticipated that either a more robust optical coupling strategy, or a defined correlation between the change of the laser signal vs. the movement of the fiber-optic cable should be integrated into the multivariate model for compensation. Last but not least, efficient mode mixing ensuring that all possible modes propagating inside the fiber are populated are a focus of future device optimization. A full fiber illumination also leads to more efficient coupling into the diamond ATR sensing element and avoids spatially distributed hotspots of the evanescent field for each laser, thus avoiding the problem that the individual lasers scan slightly different spots on the sample surface (see supplementary information).

Besides, the quantity of discarded data can be significantly reduced if the structure of the probe tip is improved towards a conical shape. The 3 mm wide cylindrical shaft of the ATR probe tip was non-ideal for measuring 4 mm cartilage samples, because the cartilage samples had varying surface structures. Illustrations of the most common cartilage plug types and the basic as well as the effects that could be observed within the measured data are highlighted in the supplementary information. Especially concave cartilage surfaces or samples where the cartilage surface and bone surface are strongly non-parallelly aligned might be damaged during measurements under higher contact pressures, because the cylindrical probe tip acts more like a stamp. Therefore, a conical probe tip would simplify the handling of different cartilage structures due to a smaller and more punctual contact area, which would provide significantly less shear forces on the observed cartilage tissue. Furthermore, potentially induced damage would be limited, and slippage of the IR-ATR probe prevented. The various structures of cartilage surface and possible associated probe tip-specific effects within the measurements were the reason for only examining the median values. Possible
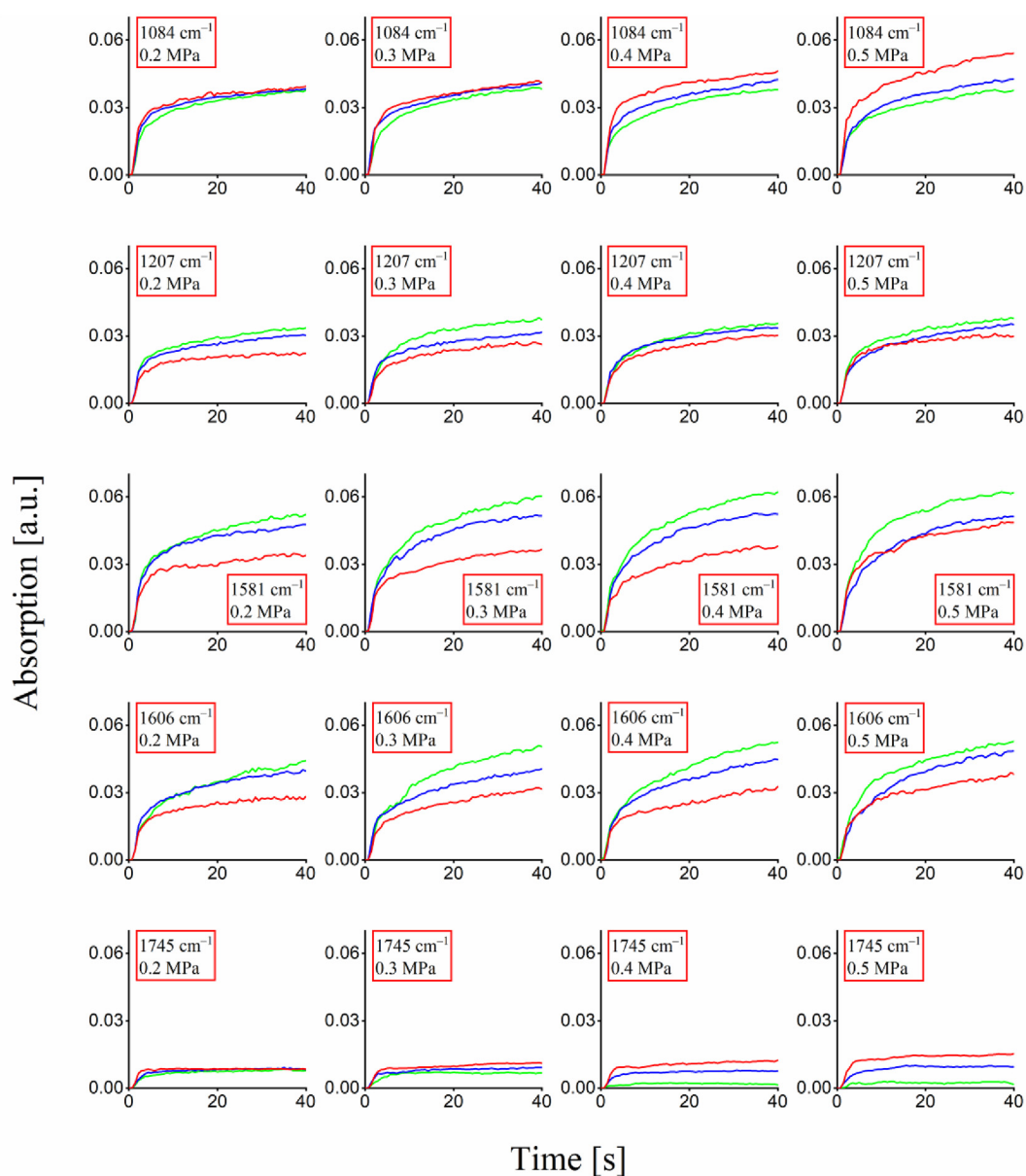
Fig. 3. Median progressions curves of healthy (green), intermediate (blue), and damaged (red) human articular cartilage tissue shown on carbohydrate (1084 cm^{-1}), amide III (1207 cm^{-1}), amide II/water (1581 cm^{-1}), amide I/water (1606 cm^{-1}) and lipid (1745 cm^{-1}) IR features.

Table 2

Distribution of the cartilage samples according to their OARSI grading results and their classification within this study.

OARSI grade	Number of AC tissue samples	Classification in this work
0	0	Healthy
1	2	Healthy
1.5	14	Healthy
2	10	Intermediate
2.5	13	Intermediate
3	0	Damaged
3.5	2	Damaged
4	7	Damaged
4.5	6	Damaged

outliers, which remained in the used data set were therefore not of great significance [38].

From the preparative side, there is also potential for improvements. Unfortunately, the cadavers from which the cartilage samples were extracted provided a very low portion of pristine cartilage tissue samples (OARSI grade 0 or 1). The distribution of samples within the OARSI grading system and the related health condition groups are presented in Table 2. Therefore, the signal differences between intermediate and healthy cartilage tissue could be even more significant than shown in this preliminary study, when the content of ideal cartilage tissue within the data set can be increased. An equal distribution of healthy, intermediate and damaged cartilage tissue is desired, because this would provide an ideal basis for chemometric or machine-learning based evaluation methods, which is required due to the dynamic nature of the spectral information that has to be analyzed in case of cartilage tissue.

The relevance of the lipid signal for assessing the cartilage condition needs to undergo further investigation in subsequent studies. It may indicate, however, that the preparation and control of the cartilage surface must be more strictly controlled in the case of very surface-sensitive ATR spectroscopy.

Furthermore, the measurement experiment can be optimized towards arthroscopic surgery in subsequent studies. Following experiments should be carried out under RS flushing, since it can be assumed that such flushing has an influence on the cartilage surface when cartilage lubricant is removed from the cartilage surface.

In summary, a prototype infrared attenuated total reflection (IR-ATR) spectroscopic arthroscopic probing system for the classification of human cartilage health condition was developed and tested *in vitro* providing promising results on the utility of the selected approach. The use of distributed feedback quantum-cascade lasers (DBF-QCLs) emitting at selected relevant wavelengths characteristic for pathological molecular changes in cartilage composition is sufficient to identify distinct spectral trends allowing for the differentiation of cartilage health states. Besides, the high temporal resolution of the lasers-based IR measurements allows for close to real-time analysis, which is mandatory for future clinical applications in arthroscopic surgery scenarios providing immediate feedback on the cartilage status. However, while the obtained results are convincing, they are based on a set of mainly degenerated samples and only handful of healthy cartilage tissue samples. Hence, it is anticipated that further augmented data sets will further amplify those differences leading to optimized classification results.

Finally, the IR probe tip will be further evolved and optimized advancing the fidelity of the analysis at different cartilage surface structures along with an improved and more robust signal propagation between the analyzer module and the arthroscopic ATR-probe better suited for "hand-held" usage during clinical applications. Nonetheless, the obtained fundamental results shown herein promise the future opportunity of diagnosing OA with the developed OA scanner system and justifies the evolution of the present system into a device that can be tested at real-world clinical conditions.

Author contributions

P. Krebs: Methodology, Device optimization, Spectral data collection, Spectral analysis, Writing – original draft.

M. Nägele: Methodology, Device development (Main unit), Device optimization, Software, Project administration, Writing/review & editing.

P. Fomina: Methodology, Device optimization, Spectral data collection.

V. Virtanen: Methodology, Pre-Studies for device development, Histological data collection, Writing/review & editing.

E. Nippolainen: Methodology, Pre-Studies for device development, Sample preparation, Writing/review & editing.

R. Shaikh: Methodology, Pre-Studies for device development, Sample preparation, Writing/review & editing.

I.O. Afara: Resources, Conceptualization, Project administration, Funding acquisition.

J. Töyräs: Resources, Conceptualization, Project administration, Funding acquisition, Writing/review & editing.

I. Usenov: Device development (Fiber-Spider & Probe).

T. Sakharova: Device development (Fiber-Spider & Probe).

V. Artyushenko: Device development (Fiber-Spider & Probe), Writing/review & editing.

V. Tafintseva: Methodology, Pre-studies for device development, Writing/review & editing.

J. H. Solheim: Methodology, Pre-studies for device development, Writing/review & editing.

B. Zimmermann: Methodology, Pre-studies for device development, Writing/review & editing.

A. Kohler: Methodology, Resources, Project administration, Funding acquisition.

O. König: Device development (Laser), Writing/review & editing.

S. Saarakkala: Conceptualization, Histological data collection, Project administration, Funding acquisition, Writing – review & editing.

B. Mizaikoff: Conceptualization, Resources, Writing – review & editing, Supervision, Project administration, Funding acquisition.

Conflicts of interest

Acknowledgement

Appendix A. Supplementary data

Supplementary data to this article can be found online at https://doi.org/10.1016/j.ocarto.2024.100466.

References

[1] N. Arden, M.C. Nevitt, Osteoarthritis: epidemiology, Best Pract. Res. Clin. Rheumatol. 20 (2006) 3–25.

[2] L. March, M. Cross, C. Lo, N.K. Arden, L. Gates, K.M. Leyland, et al., Osteoarthritis: A Serious Disease: Submitted to the U.S. Food and Drug Administration. https://www.oarsi.org/sites/default/files/docs/2016/oarsi_white_paper_oa_serious_disease_121416_1.pdf.

[3] R. Shaikh, E. Nippolainen, V. Virtanen, J. Torniainen, L. Rieppo, S. Saarakkala, et al., Raman spectroscopy is sensitive to biochemical changes related to various cartilage injuries, J. Raman Spectrosc. 52 (2021) 796–804.

[4] W. Zhang, H. Ouyang, C.R. Dass, J. Xu, Current research on pharmacologic and regenerative therapies for osteoarthritis, Bone Res. 4 (2016) 15040.

[5] L. Ryd, M. Brittberg, K. Eriksson, J.S. Jurvelin, A. Lindahl, S. Marlovits, et al., Pre-osteoarthritis, Cartilage 6 (2015) 156–165.

[6] C.R. Chu, A.A. Williams, C.H. Coyle, M.E. Bowers, Early diagnosis to enable early treatment of pre-osteoarthritis, Arthritis Res. Ther. 14 (2012) 212.

[7] H.J. Braun, G.E. Gold, Diagnosis of osteoarthritis: imaging, Bone 51 (2012) 278–288.

[8] F. Eckstein, F. Cicuttini, J.P. Raynauld, J.C. Waterton, C. Peterfy, Magnetic resonance imaging (MRI) of articular cartilage in knee osteoarthritis (OA): morphological assessment, Osteoarthritis Cartilage 14 (2006) 46–75.

[9] M.D. Iversen, L.L. Price, J. Von Heideken, W.F. Harvey, C. Wang, Physical examination findings and their relationship with performance-based function in adults with knee osteoarthritis, BMC Muscoskel. Disord. 17 (2016) 273.

[10] J. Favre, B.M. Jolles, Gait analysis of patients with knee osteoarthritis highlights a pathological mechanical pathway and provides a basis for therapeutic interventions, EFORT Open Rev 1 (2016) 368–374.

[11] V. Bousson, T. Lowitz, L. Laouisset, K. Engelke, J.-D. Laredo, CT imaging for the investigation of subchondral bone in knee osteoarthritis, Osteoporos. Int. 23 (2012) 861–865.

[12] L. de Girolamo, E. Kon, G. Filardo, A.G. Marmotti, F. Soler, G.M. Peretti, et al., Regenerative approaches for the treatment of early OA, Knee Surg. Sports Traumatol. Arthrosc. 24 (2016) 1826–1835.

[13] A.E. Weber, I.K. Bolia, N.A. Trasolini, Biological strategies for osteoarthritis: from early diagnosis to treatment, Int. Orthop. 45 (2021) 335–344.

[14] R.L. Taruc-Uy, S.A. Lynch, Diagnosis and Treatment of Osteoarthritis, Primary Care - Clinics in Office Practice 40 (2013) 821–836.

[15] P. Niemeyer, M.J. Feucht, J. Fritz, D. Albrecht, G. Spahn, P. Angele, Cartilage repair surgery for full-thickness defects of the knee in Germany: indications and epidemiological data from the German Cartilage Registry (KnorpelRegister DGOU), Arch. Orthop. Trauma Surg. 136 (2016) 891–897.

[16] A.H. Gomoll, T. Minas, The quality of healing: articular cartilage, Wound Repair Regen. 22 (2014) 30–38.

[17] V. Virtanen, V. Tafintseva, R. Shaikh, E. Nippolainen, J. Haas, I.O. Afara, et al., Infrared spectroscopy is suitable for objective assessment of articular cartilage health, Osteoarthr Cartil Open 4 (2022) 100250.

[18] M. Paraskevaidi, P.L. Martin-Hirsch, F.L. Martin, ATR-FTIR spectroscopy tools for medical diagnosis and disease investigation, in: C. Kumar (Ed.), Nanotechnology Characterization Tools for Biosensing and Medical Diagnosis, Springer, Berlin, Heidelberg, 2018.

[19] P.J. Larkin, Infrared and Raman Spectroscopy, Elsevier, 2011.

[20] S.E. Glassford, B. Byrne, S.G. Kazarian, Recent applications of ATR FTIR spectroscopy and imaging to proteins, Biochim. Biophys. Acta, Proteins Proteomics 1834 (2013) 2849–2858.

[21] J. Haas, R. Stach, M. Sieger, Z. Gashi, M. Godejohann, B. Mizaikoff, Sensing chlorinated hydrocarbons via miniaturized GaAs/AlGaAs thin-film waveguide flow cells coupled to quantum cascade lasers, Anal. Methods 8 (2016) 6602–6606.

[22] P.R. Griffiths, J.A. de Haseth, Fourier Transform Infrared Spectrometry, John Wiley & Sons, Inc., 2007.

[23] J. Haas, B. Mizaikoff, Advances in mid-infrared spectroscopy for chemical analysis, Annu. Rev. Anal. Chem. 9 (2016) 45–68.

[24] R. Karoui, G. Downey, C. Blecker, Mid-infrared spectroscopy coupled with chemometrics: a tool for the analysis of intact food systems and the exploration of their molecular Structure−Quality relationships − A review, Chem. Rev. 110 (2010) 6144–6168.

[25] A. Kohler, N.K. Afseth, H. Martens, Chemometrics in biospectroscopy, in: Handbook of vibrational spectroscopy, John Wiley & Sons, Ltd, 2010.

[26] A.J. Sophia Fox, A. Bedi, S.A. Rodeo, The basic science of articular cartilage: structure, composition, and function, Sport Health 1 (2009) 461–468.

[27] S. Lohmander, Proteoglycans of joint cartilage, Bailliere's Clin. Rheumatol. 2 (1988) 37–62.

[28] L. Lippiello, T. Walsh, M. Fienhold, The association of lipid abnormalities with tissue pathology in human osteoarthritic articular cartilage, Metabolism 40 (1991) 571–576.

[29] H.U. Rehman, V. Tafintseva, B. Zimmermann, J.H. Solheim, V. Virtanen, R. Shaikh, et al., Preclassification of broadband and sparse infrared data by multiplicative signal correction approach, Molecules 27 (2022) 2298.

[30] N.P. Camacho, P. West, P.A. Torzilli, R. Mendelsohn, FTIR microscopic imaging of collagen and proteoglycan in bovine cartilage, Biopolymers 62 (2001) 1–8.

[31] L. Rieppo, J. Töyräs, S. Saarakkala, Vibrational spectroscopy of articular cartilage, Appl. Spectrosc. Rev. 52 (2017) 249–266.

[32] J.-B. Brubach, A. Mermet, A. Filabozzi, A. Gerschel, P. Roy, Signatures of the hydrogen bonding in the infrared bands of water, J. Chem. Phys. 122 (2005) 184509.

[33] F.O. Libnau, J. Toft, A.A. Christy, O.M. Kvalheim, Structure of liquid water determined from infrared temperature profiling and evolutionary curve resolution, J. Am. Chem. Soc. 116 (1994) 8311–8316.

[34] F. Stärke, F. Awiszus, C.H. Lohmann, C. Stärke, The effect of irrigation time and type of irrigation fluid on cartilage surface friction, J. Mech. Behav. Biomed. Mater. 77 (2018) 187–191.

[35] W. Waldstein, G. Perino, S.L. Gilbert, S.A. Maher, R. Windhager, F. Boettner, OARSI osteoarthritis cartilage histopathology assessment system: a biomechanical evaluation in the human knee, J. Orthop. Res. 34 (2016) 135–140.

[36] L.P. Li, W. Herzog, R.K. Korhonen, J.S. Jurvelin, The role of viscoelasticity of collagen fibers in articular cartilage: axial tension versus compression, Med. Eng. Phys. 27 (2005) 51–57.

[37] L. Edelsten, J.E. Jeffrey, L.V. Burgin, R.M. Aspden, Viscoelastic deformation of articular cartilage during impact loading, Soft Matter 6 (2010) 5206.

[38] M. Qi, Z. Fu, F. Chen, Outliers detection method of multiple measuring points of parameters in power plant units, Appl. Therm. Eng. 85 (2015) 297–303.